Open Access, Peer Reviewed, Research Journal

Print & Online available on https://jesbulletin.in
Research Article

Synthesis of $ZnFe_2O_4$ SMNPs via Sol-Gel Auto-Combustion: Structural, Magnetic, and Electrical Characterization

Jagruti Shripatrao Bansode [a*], *Pramod Humbad* [a], *Archana Chapolikar* [b], *V.D. Murumkar* [c], *Sangita Shinde* [d]

[a]*Department of Physics, JES College, Jalna 431203 INDIA*
[b]*Department of Chemistry, Government College of Arts Commercce and Science, Chhatrapti Sambhajinagar 431001 INDIA*
[c]*Department of Physics, Vivekanand Arts, Sardar DalipSingh Commerce and Science College, Chhatrapti Sambhajinagar 431001 INDIA*

Corresponding author:

ARTICLE INFO

Received: 10/02/2024
Revised: 15/03/2024
Accepted: 01/04/2024

KEYWORDS

SMNPs; Solgel; *IR* spectroscopy; magnetic property; DC-Electrical property

ABSTRACT

The $ZnFe_2O_4$ magnetic nanoparticles (SMNPs) were synthesized successfully using the sol-gel auto-combustion method, with citric acid ($C_6H_8O_7$) serving as the fuel. X-ray diffraction (XRD) analysis confirmed the formation of a cubic spinel structure belonging to the $Fd3m - Oh7$ space group, with a lattice constant (a) of 8.4 ± 0.05 Å. The average crystallite size (t), determined using Debye-Scherrer's method from peak broadening, was approximately 36 nm. Fourier-transform infrared (FT-IR) spectroscopy identified the 2 characteristic metal-oxide bands at $\sim 550\ cm^{-1}$ (O-M Oct) and $\sim 400\ cm^{-1}$ (O-M Td), corresponds to the Octahedral and tetrahedral metal-oxygen bonds, respectively, confirming the structural integrity of the synthesized material. Magnetic measurements indicated the saturation magnetization (Ms); a remanent magnetization (Mr) and a magneton number (nB). The DC electrical resistivity measurements, following the Arrhenius equation, demonstrated the semiconducting nature of the $ZnFe_2O_4$ SMNPs.

1 Introduction

Spinel Magnetic Zinc ferrite nanoparticles ($ZnFe_2O_4$ SMNPs) are a class of magnetic nanomaterials with a unique confluence of properties that position them as promising candidates for a diverse array of advanced technological applications [1]. At the core of their functionality lies their inherent ferrimagnetism, a phenomenon arising from the antiparallel alignment of magnetic moments within the spinel crystal structure, resulting in a net magnetic moment [2]. This intrinsic magnetic behavior, coupled with their nanoscale dimensions, renders them highly susceptible to external magnetic fields, enabling precise manipulation and control for targeted applications such as magnetic drug delivery, hyperthermia treatment, and magnetic resonance imaging (MRI) contrast agents [3]. $ZnFe_2O_4$ nanoparticles (SMNPs) possess exceptional characteristics that render them highly applicable across various technological fields. These include their use in soft magnetic materials, components with low losses for high-frequency applications, gas sensors, semiconductor photocatalysts, and energy conversion devices such as magnetocaloric pumps [4]. Recent studies have highlighted the effectiveness of $ZnFe_2O_4$ SMNPs in gas-sensing technologies, showcasing their heightened sensitivity to gases like methane (CH_4), hydrogen sulfide (H_2S), liquefied petroleum gas (LPG), and ethanol (C_2H_5OH) [5]. Such properties underscore the importance of $ZnFe_2O_4$ SMNPs in environmental monitoring and industrial gas detection, illustrating their versatility in both scientific and industrial applications. $ZnFe_2O_4$ SMNPs exhibit exceptional chemical stability, demonstrating remarkable resistance to degradation in a wide range of chemical environments, including corrosive media and high temperatures. This inherent robustness makes them suitable for deployment in demanding applications such as environmental remediation; where they can be acted an efficient catalyst for the degradation of pollutants, and in energy storage devices, where their stability enhances their electrochemical performance [6]. The diminutive size of these SMNPs translates into a significantly elevated surface area-to-volume ratio, a critical factor that amplifies their reactivity and catalytic activity. Beyond their

magnetic and catalytic attributes, $ZnFe_2O_4$ SMNPs exhibit intriguing optical properties. They demonstrate strong absorption of light within the visible and near-infrared regions of the electromagnetic spectrum, a characteristic that makes them potential candidates for integration into optoelectronic devices such as photodetectors and solar cells. This unique amalgamation of magnetic, chemical, and optical properties establishes $ZnFe_2O_4$ SMNPs as versatile materials with the potential to revolutionize various fields, including data storage, catalysis [7], environmental remediation [8], energy conversion, and biomedical applications [9].

Spinel ferrites, described by the general formula $MeFe_2O_4$ (where Me represents divalent cations such as $Fe^{2+}, Co^{2+}, Ni^{2+}, Cu^{2+}, Mg^{2+}, or\ Zn^{2+}$), have attracted considerable attention from researchers due to their exceptional combination of electromagnetic properties, chemical stability, mechanical strength, and adjustable magnetic characteristics [10]. Among these, zinc ferrite ($ZnFe_2O_4$) SMNPs have been extensively studied for their high electromagnetic performance, low coercivity, moderate saturation magnetization, and excellent stability. In this research article, $ZnFe_2O_4$ SMNPs were synthesized via the sol-gel auto-combustion method; which is noted for its simplicity, cost efficiency, and ability to produce SMNPs with excellent chemical homogeneity and physical uniformity. The sol-gel auto combustion approach provides significant benefits over alternative synthesis techniques by allowing optimal molecular mixing of precursor materials, leading to uniform SMNPs with precisely controlled size and morphology [11].

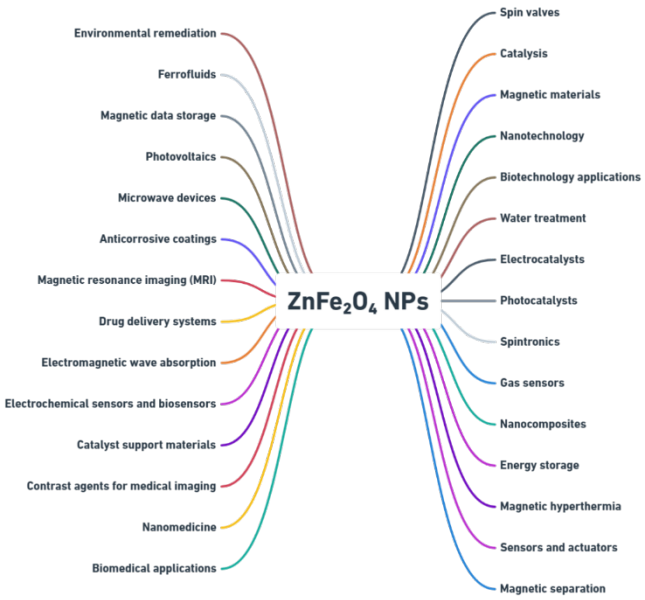

Figure 1. Various applications of ZnFe₂O₄ SMNPs

This method guarantees the creation of $ZnFe_2O_4$ SMNPs with high purity and structural integrity. This extensive study investigates how the sol-gel auto-combustion technique affects the structural and magnetic properties of $ZnFe_2O_4$ SMNPs. The capacity to manage and enhance the physical characteristics of $ZnFe_2O_4$ SMNPs via sol-gel synthesis and subsequent characterization techniques holds significant promise for developing advanced materials with tailored functionalities. Such innovations could be crucial in emerging technologies, including magnetic data storage, catalysis, gas sensing, and biomedical applications. The advancements in the synthesis and characterization of spinel ferrites like $ZnFe_2O_4$ are anticipated to expand their use in novel industrial and technological solutions.

2. Experimental

2.1 Materials

AR-grade (Analytical Reagent grade) chemicals procured from Fisher Scientific Pvt Ltd were utilized for the synthesis process to ensure precision, consistency, and reliability in experimental outcomes. These high-purity reagents, with a purity level of 99.9%, were specifically chosen to meet the rigorous demands of advanced research and laboratory instrumentation. The chemicals employed in the study included ferrous nitrate ($Fe(NO_3)_3 \cdot 9H_2O$), zinc nitrate ($Zn(NO_3)_2 \cdot 6H_2O$), citric acid ($C_6H_8O_7$), ammonia solution ($NaOH$), and deionized water, each serving a critical function in the synthesis process. Ferrous nitrate provided the primary source of iron ions, while zinc nitrate supplied zinc ions. Citric acid acted as a chelating agent, ensuring uniform mixing of metal ions through the formation of metal-citrate complexes. The ammonia solution was used to adjust the pH, facilitating the controlled precipitation of metal hydroxides, and deionized water was employed as a solvent to eliminate potential impurities. The reagents were used without further purification to maintain the integrity of the synthesis process, ensuring high reproducibility and accurate results. The selection of such high-purity chemicals minimized contamination risks and unwanted side reactions that could affect the properties of the synthesized material. By adhering to stringent standards in the selection and use of reagents, this study ensured reliable and reproducible data, emphasizing the importance of chemical quality and experimental rigor in the synthesis of advanced materials.

2.2 Synthesis of $ZnFe_2O_4$ SMNPs

ZnFe₂O₄ SMNPs were synthesized using a sol-gel auto-combustion method with stoichiometric amounts of analytical reagent-grade ferric nitrate ($Fe(NO_3)_3 \cdot 9H_2O$) and zinc nitrate ($Zn(NO_3)_2$) of 99.9% purity. The metal ions were dissolved in deionized water and complexed with citric acid ($C_6H_8O_7$) at a 1:3 molar ratio, forming a stable precursor for ferrite ceramics. The coordination bonds between the electron-deficient metal ions and the electron-rich functional groups of citric acid facilitated the sol-gel process. The solution pH was carefully adjusted to 7 using a dropwise addition of ammonia solution (NH_3), which was critical for optimizing the structural integrity of the precursor and controlling the combustion characteristics during the auto-combustion process. Maintaining this pH also contributed to the development of a porous precursor structure, essential for enhancing the auto-combustion behavior. The mixed metal nitrate solution was heated

and stirred continuously on a magnetic hotplate stirrer at $70-80°C$ until it transitioned into a dried gel during the evaporation stage. The solution gradually thickened, turning viscous and brown before forming a sticky gel. This gel underwent spontaneous combustion, producing a glowing flame that resulted in a fluffy, loose powder of pre-sintered zinc ferrite. The exothermic redox reaction between the oxidants (nitrates) and the reductant (citric acid) facilitated the formation of a ferrite-phased, ash-like material, which was subsequently dried and ground into a fine powder. The slow cooling to room temperature at the same rate enhanced crystallinity, minimized particle agglomeration, and promoted the formation of phase-pure $ZnFe_2O_4$ while reducing impurity phases. The annealed powder was then finely ground using a mortar and pestle under dry conditions to ensure uniformity in particle size. Finally, disc-shaped pellets ($10\,mm$ in diameter and $3\,mm$ in height) were fabricated using a hydraulic press by applying a pressure of $5\,tons/cm^2$ for 5 minutes. This environmentally friendly synthesis route highlights the potential of sol-gel auto-combustion as an efficient and scalable method for producing high-purity $ZnFe_2O_4$ SMNPs.

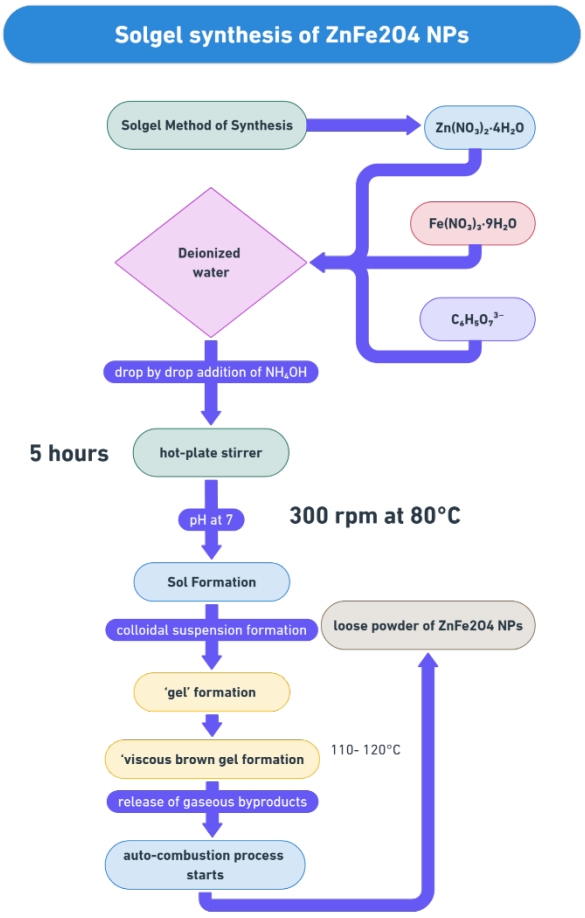

Figure 1 schematic overview of sol-gel auto-combustion synthesis process of $ZnFe_2O_4$ SMNPs.

2.3 Characterizations of $ZnFe_2O_4$ SMNPs

To comprehensively characterize the synthesized $ZnFe_2O_4$ SMNPs; a combination of analytical techniques was employed. X-ray diffraction (XRD) analysis, performed at room temperature ($28-33°C$) using a Bruker D-8 diffractometer with $Cu-K\alpha$ radiation, confirmed the formation of the desired spinel structure and identified any potential impurities. Fourier Transform Infrared (FT-IR) spectroscopy provided insights into the chemical bonding and functional groups present within the SMNPs, revealing information about metal-oxygen bonds and residual organic components. Magnetic properties were evaluated using a pulse-field hysteresis loop tracer, providing crucial data on coercivity, remanence, and saturation magnetization. To assess their electrical behavior, DC-electrical resistivity measurements were conducted on pelletized samples using a two-probe method. The combined application of XRD, FT-IR, magnetic hysteresis measurements, and DC-electrical resistivity analysis provided a comprehensive understanding of the structural, chemical, magnetic, and electrical properties of the synthesized $ZnFe_2O_4$ SMNPs, confirming the successful synthesis of high-quality SMNPs and validating the efficacy of the sol-gel auto-combustion method. These findings lay the groundwork for further exploration of their potential in advanced technological applications.

3 Results and discussion

3.1 X-ray diffraction of $ZnFe_2O_4$ SMNPs

X-ray diffraction (XRD) patterns of $ZnFe_2O_4$ SMNPs were acquired using a Model X'PertPRO MPD PANalytical system at room temperature, both before and after exposure to 100 kGy of gamma irradiation. Data was collected over a 2θ range of 20° to 80° using $Cu-K\alpha$ radiation ($\lambda = 1.5405$ Å) with a step size of 0.02° and a 1 −second count time per step, resulting in a total data acquisition time of 3 hours. The observed Bragg reflections were compared to the $JCPDS$ card number $22-1012$ [12] to confirm the presence of a single-phase $ZnFe_2O_4$ with a face-centered cubic spinel structure. XRD analysis is crucial for differentiating between size-induced and strain-induced broadening of diffraction peaks, which can be effectively analyzed by fitting Lorentzian and Gaussian profiles to characteristic peaks such as (220) and (440). Figure 2 illustrates the XRD pattern of $ZnFe_2O_4$ magnetic SMNPs synthesized via the sol-gel auto-combustion method at room temperature, covering a (2θ) range of $20°-80°$. The X-ray diffraction (XRD) pattern confirms the successful synthesis of crystalline zinc ferrite $(ZnFe_2O_4)$ SMNPs with a cubic spinel structure. Sharp and distinct diffraction peaks, indexed by Miller indices such as $(311), (220), (400), (422), (511), (440), and\ (622)$, [13] are observed, indicating a well-defined crystal structure. The most intense peak, corresponding to the (311) plane, is characteristic of spinel ferrites. The absence of any secondary peaks in the XRD pattern confirms the phase purity of the synthesized sample, indicating the absence of detectable impurities. These results collectively demonstrate the successful formation of a single-phase, highly crystalline zinc ferrite [16]. The formula for lattice constant was;

$$a = d_{hkl}\sqrt{h^2 + k^2 + l^2} \quad (1)$$

where d is the interplanar spacing, a is the lattice constant, and hkl are the Miller indices of each plane in the family. The lattice parameter value for $ZnFe_2O_4$ SMNPs was determined using the Debye-Scherrer formula [20, 21];

$$D = \frac{k\lambda}{\beta \cos\theta} \quad (2)$$

Here, k is a constant with a value of 0.89, λ is the wavelength of the X-ray source (1.5405 Å), β represents the full width at half maximum ($FWHM$), and θ is the glancing angle.

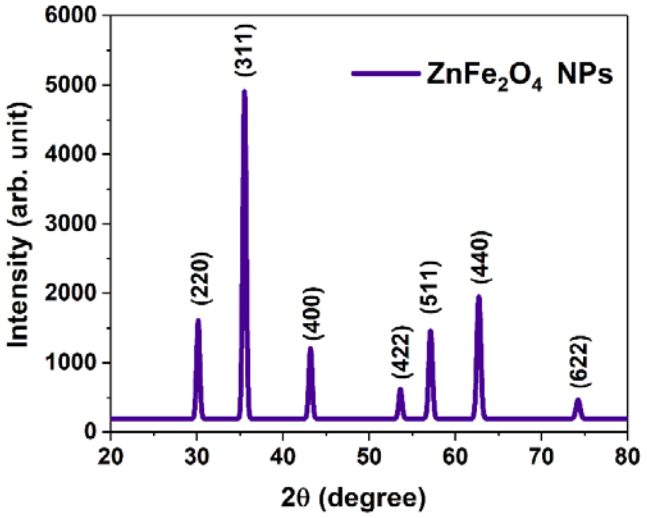

Figure 2 X-ray diffraction (XRD) pattern of $ZnFe_2O_4$ SMNPs

This confirms the formation of a well-structured cubic spinel crystal with minimal distortions. These results indicate that the SMNPs exhibit high crystalline quality, aligning with the expected properties of ferrite materials. The observed decrease in d-spacing with increasing Bragg's angle follows standard crystallographic behavior, validating the accuracy of the measurements and the integrity of the synthesized material. Based on this relationship, the X-ray density (dx) of $ZnFe_2O_4$ SMNPs was calculated using the formula:

$$d_x = {}^{8M}/_{N_A a^3} \quad (3)$$

where d_x is the X-ray density, M is the relative molecular weight of the composition, N_A is Avogadro's number, and aaa is the lattice constant. The factor 8 reflects the presence of eight formula units per unit cell. The bulk density (dB) of the samples was determined using Archimedes' principle. The distances between magnetic ions, referred to as hopping lengths (L_A and L_B) at the tetrahedral (A) and octahedral (B) sites, were calculated using the appropriate relations [24, 25].

$$L_A = {}^{a\sqrt{3}}/_{4} \quad (4)$$

$$L_B = {}^{a\sqrt{2}}/_{4} \quad (5)$$

3.2 FTIR of $ZnFe_2O_4$ SMNPs

The **Figure 3** presents the FTIR spectrum of $ZnFe_2O_4$ magnetic SMNPs (SMNPs) recorded at room temperature in the range of 350-4000 cm⁻¹. Spinel ferrites typically exhibit two characteristic absorption bands in the FTIR spectra within the 370-600 cm⁻¹ region, attributed to metal-oxygen ($M-O$) stretching vibrations. In the $ZnFe_2O_4$ SMNPs, the higher wavenumber band at approx. 550 cm^{-1}; ($v1$) corresponds to $M-O$ stretching vibrations at the tetrahedral (A) site of the spinel lattice, where the metal-oxygen bond is shorter. Conversely, the lower wavenumber band close to 400 cm^{-1} ($v2$) is associated with $M-O$ stretching vibrations at the octahedral (B) site; characterized by a slightly longer metal-oxygen bond. These two distinct absorption bands serve as a characteristic "fingerprint" for spinel ferrites, providing valuable insights into their crystal structure and the bonding environment of metal ions within the lattice [27, 28]. The observed variations in bond lengths between the tetrahedral (A) and octahedral (B) sites significantly influence their vibrational frequencies. The shorter oxygen-iron bond length (1.89 Å) at the tetrahedral site results in stronger covalent bonding and consequently higher vibrational stretching frequencies compared to the longer oxygen-iron bond (1.99 Å) at the octahedral site, where weaker bonding leads to lower frequencies. This distinct vibrational behavior is a characteristic feature of spinel structures, arising from the specific arrangement of cations within tetrahedral and octahedral voids. The presence of two distinct interstitial stretching modes, $v1$ and $v2$, in the FTIR spectrum directly confirms the spinel structure of $ZnFe_2O_4$ SMNPs. These modes are characteristic of the spinel lattice, where the unique geometric arrangement of metal ions in tetrahedral and octahedral sites gives rise to these specific vibrational patterns. The clear differentiation between these vibrational modes in the FTIR spectrum further validates the material's spinel configuration. This phenomenon is not unique to $ZnFe_2O_4$ but is a hallmark of spinel ferrites, where subtle variations in bond lengths and coordination environments result in complex vibrational patterns. These seemingly small structural differences have significant implications for the material's overall properties, including its magnetic, electrical, and catalytic behaviors. The complexity observed in the FTIR spectrum reflects intricate molecular-level interactions within the material. This intricacy echoes Richard Feynman's observation that "the beauty of a flower may not be just in its color, but in the complexity it reveals. Similarly, in $ZnFe_2O_4$ and other ferrites, the true elegance

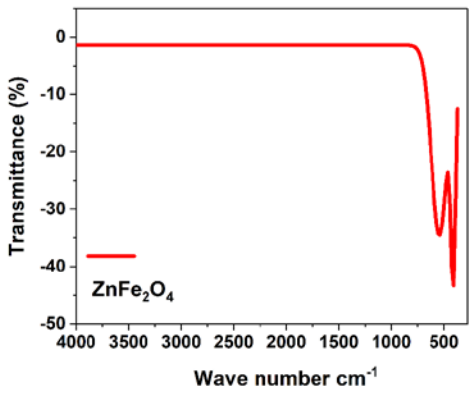

Figure 3 FTIR spectra of $ZnFe_2O_4$ SMNPs

3.3 Magnetic property of $ZnFe_2O_4$ SMNPs

The Magnetic properties of $ZnFe_2O_4$ samples, including saturation magnetization (Ms), remanent magnetization (Mr), coercivity (Hc), squareness ratio (Mr/Ms), and magneton number (nB), were determined using Pulse-Field Hysteresis Loop ($PFHL$) measurements (**Figure 4**). The measured Ms and Mr suggest a disruption of exchange interactions at the nanoparticle surfaces, leading to surface-canted spins. The observed coercivity (Hc) is likely attributed to nanoscale size effects, influencing domain wall pinning and surface anisotropies. The squareness ratio (Mr/Ms) indicates a mixed multi-domain and single-domain magnetic behavior. In the inverted spinel structure of $ZnFe_2O_4$, Co^{2+} ions at the octahedral (B) sites contribute a magnetic moment, while the magnetic moments of Fe^{3+} ions at both tetrahedral (A) and octahedral (B) sites largely cancel each other due to antiferromagnetic coupling. The calculated magneton number (nB) per formula unit, suggests moderate $A-B$ site interaction, consistent with the typical magnetic behavior observed in spinel ferrites [31][33, 34].

$$n_B = \frac{[M_S \times M_W]}{5585} \quad (6)$$

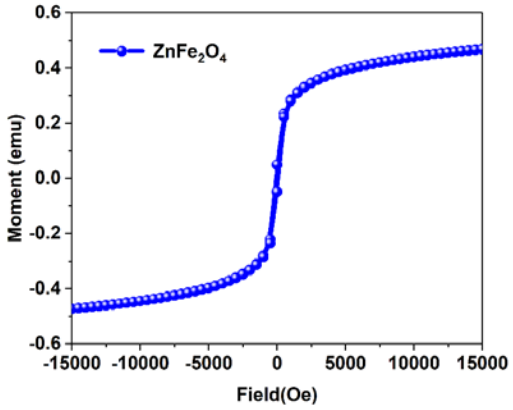

Figure 4 *Hysteresis loop of $ZnFe_2O_4$ SMNPs*

The surface anisotropy and spin canting, arising from reduced coordination and altered exchange interactions at the nanoparticle surface, contributed to a decrease in saturation magnetization and influenced the magnetic hysteresis behavior. These findings, consistent with theoretical predictions, underscore the significant impact of particle size, surface structural features, and synthesis conditions on the magnetic properties of $ZnFe_2O_4$ SMNPs.

3.4 DC-resistivity of $ZnFe_2O_4$ SMNPs

The Zinc ferrite exhibits high resistivity, exceeding $10^9\ \Omega \cdot cm$, classifying it as a highly resistive material. As shown in **Figure 5**, the DC resistivity of $ZnFe_2O_4$ SMNPs decreases with increasing temperature, characteristic of a conduction mechanism dominated by weak polaron hopping between Fe^{2+} and Fe^{3+} ions. This temperature dependence confirms the semiconducting nature of $ZnFe_2O_4$ SMNPs. For characterization, the nanopowder was compressed into a $10\ mm$ diameter, $2\ mm$ thick pellet using a KBr press.

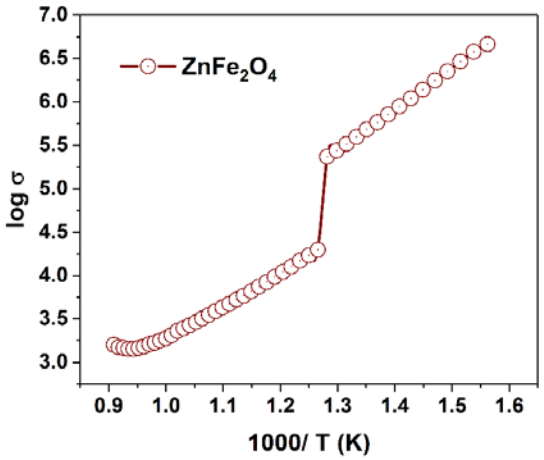

Figure 5 *DC-electrical resistivity of $ZnFe_2O_4$ SMNPs*

To ensure the reliable electrical contact, a thin layer of silver paste was applied to both sides of the pellet. The temperature-dependent DC resistivity was subsequently measured over the temperature range of 300-600 °C using a two-probe method. The DC resistivity of spinel ferrites is influenced by various factors, including the concentration of Fe^{2+} ions at octahedral (B) sites, grain size (G), sintering temperature, and porosity ($P\%$). The electrical resistivity (ρ) was determined using the Arrhenius relation, which describes the temperature (T) dependence of DC resistivity [35];

$$\rho = \rho_0 \times \exp\left(\frac{\Delta E_a}{kT}\right) \quad (7)$$

The Arrhenius equation, $\rho = \rho_0\, exp(Ea/kT)$, describes the temperature dependence of DC resistivity, where ρ_0 is the temperature-independent resistivity, Ea is the activation energy, k is the Boltzmann constant, and T is the absolute temperature. The activation energy (Ea), determined to be in between $2.5-3.5\ eV$, governs the temperature-dependent mobility of charge carriers within the ferrite material. According to the Arrhenius relation, electrical resistivity decreases with increasing temperature, a characteristic behavior of semiconductors. In $ZnFe_2O_4$ SMNPs, this decrease in resistivity arises from an enhancement in charge carrier mobility at elevated temperatures. As temperature increases, more charge carriers acquire sufficient energy to overcome potential barriers, resulting in increased mobility and a corresponding decrease in resistivity;

$$\mu = 1/ne\rho \quad (8)$$

where μ is the mobility, e is the electronic charge, ρ is the resistivity, and n is the charge carrier concentration. The charge carrier concentration (n) can be calculated using the equation:

$$n = \frac{Na\rho P}{M_W} \quad (9)$$

where M_W is the molecular weight, NA is Avogadro's number, ρ is the sample density, and P represents the number of iron atoms in the oxide's chemical formula.

4. Conclusions

The The sol-gel auto-combustion technique was effectively employed to synthesize $ZnFe_2O_4$ magnetic nanoparticles (SMNPs), with citric acid $(C_6H_8O_7)$ acting as the fuel. X-ray diffraction (XRD) analysis of the $ZnFe_2O_4$ SMNPs confirmed the formation of a cubic spinel structure, corresponding to the F_{d3m}-Oh_7 space group. The lattice constant (a) of the synthesized SMNPs was measured at $\sim 8.4 \pm 0.05$ Å. Peak broadening analysis using Debye-Scherrer's equation revealed an average crystallite size (t) in nanometer. The Fourier-transform infrared (FT-IR) spectra displayed two prominent metal-oxide bands at around $550\ cm^{-1}$ (O-M Oct) and $400\ cm^{-1}$ (O-M Td), which correspond to the metal-oxygen bonds at the octahedral and tetrahedral sites, respectively, within the $ZnFe_2O_4$ structure. These bands, which fall within the typical range of $370\ to\ 600\ cm^{-1}$ for spinel ferrites, confirmed the structural integrity of the synthesized material. Magnetic measurements showed a saturation magnetization (Ms); a remanent magnetization (Mr); and a magneton number (nB). DC electrical resistivity measurements, in agreement with the Arrhenius equation, confirmed the semiconducting nature of the $ZnFe_2O_4$ SMNPs.

Reference

[1] D.S. Mathew, R.-S. Juang, An overview of the structure and magnetism of spinel ferrite nanoparticles and their synthesis in microemulsions, Chemical engineering journal, 129 (2007) 51-65.

[2] H. Dawoud, S. Shaat, Magnetic properties of Zn substituted Cu ferrite, DOI (2006).

[3] Z. Ghasemian, D. Shahbazi-Gahrouei, S. Manouchehri, Cobalt zinc ferrite nanoparticles as a potential magnetic resonance imaging agent: An in vitro study, Avicenna journal of medical biotechnology, 7 (2015) 64.

[4] M. Qin, Q. Shuai, G. Wu, B. Zheng, Z. Wang, H. Wu, Zinc ferrite composite material with controllable morphology and its applications, Materials Science and Engineering: B, 224 (2017) 125-138.

[5] A. Singh, A. Singh, S. Singh, P. Tandon, B. Yadav, R. Yadav, Synthesis, characterization and performance of zinc ferrite nanorods for room temperature sensing applications, Journal of Alloys and Compounds, 618 (2015) 475-483.

[6] P.B. Kharat, S.B. Somvanshi, E.A. Dawi, A.M. Mopari, N.H. Bansod, Exploring the electrochemical performance of nickel-zinc ferrite nanoparticles for supercapacitor applications, Journal of Materials Science: Materials in Electronics, 35 (2024) 606.

[7] B. Anjaneyulu, Chinmay, V. Chauhan, S.A. Carabineiro, M. Afshari, Recent advances on zinc ferrite and its derivatives as the forerunner of the nanomaterials in catalytic applications, Journal of Inorganic and Organometallic Polymers and Materials, 34 (2024) 1887-1907.

[8] S. Latif, A. Liaqat, M. Imran, A. Javaid, N. Hussain, T. Jesionowski, M. Bilal, Development of zinc ferrite nanoparticles with enhanced photocatalytic performance for remediation of environmentally toxic pharmaceutical waste diclofenac sodium from wastewater, Environmental Research, 216 (2023) 114500.

[9] J. Garg, M.N. Chiu, S. Krishnan, R. Kumar, M. Rifah, P. Ahlawat, N.K. Jha, K.K. Kesari, J. Ruokolainen, P.K. Gupta, Emerging trends in zinc ferrite nanoparticles for biomedical and environmental applications, Applied Biochemistry and Biotechnology, 196 (2024) 1008-1043.

[10] A. Pradeep, P. Priyadharsini, G. Chandrasekaran, Structural, magnetic and electrical properties of nanocrystalline zinc ferrite, Journal of Alloys and Compounds, 509 (2011) 3917-3923.

[11] S. Zahi, M. Hashim, A. Daud, Synthesis, magnetic properties and microstructure of Ni–Zn ferrite by sol–gel technique, Journal of Magnetism and Magnetic Materials, 308 (2007) 177-182.

[12] U. Steinike, P. Druska, B. Wallis, D.C. Uecker, V. Sepelak, Formation and surface structure of Ti–Zn-double oxides and Zn ferrite, Chem Papers, 52 (1998) 147-151.

[13] B. Mishra, B. Munisha, J. Nanda, K. Sankaran, S. Suman, Hydrothermally Synthesized Magnesium doped Zinc Ferrite Nanoparticles: An extensive study on structural, optical, magnetic, and dielectric properties, Materials Chemistry and Physics, 292 (2022) 126791.